

# Skyrmion Dynamics in Multiferroic Insulator

Ye-Hua Liu,<sup>1</sup> You-Quan Li,<sup>1</sup> and Jung Hoon Han<sup>2,3,\*</sup>

<sup>1</sup>*Zhejiang Institute of Modern Physics and Department of Physics,  
Zhejiang University, Hangzhou 310027, People's Republic of China*

<sup>2</sup>*Department of Physics and BK21 Physics Research Division,  
Sungkyunkwan University, Suwon 440-746, Korea*

<sup>3</sup>*Asia Pacific Center for Theoretical Physics, Pohang, Gyeongbuk 790-784, Korea*

(Dated: October 31, 2018)

Recent discovery of Skyrmion crystal phase in insulating multiferroic compound  $\text{Cu}_2\text{OSeO}_3$  calls for new ways and ideas to manipulate the Skyrmions in the absence of spin transfer torque from the conduction electrons. It is shown here that the position-dependent electric field, pointed along the direction of the average induced dipole moment of the Skyrmion, can induce the Hall motion of Skyrmion with its velocity orthogonal to the field gradient. Finite Gilbert damping produces longitudinal motion. We find a rich variety of resonance modes excited by a.c. electric field.

PACS numbers: 75.85.+t, 75.70.Kw, 76.50.+g

Skyrmions are increasingly becoming commonplace sightings among spiral magnets including the metallic B20 compounds[1–5] and most recently, in a multiferroic insulator  $\text{Cu}_2\text{OSeO}_3$ [6]. Both species of compounds display similar thickness-dependent phase diagrams[5, 6] despite their completely different electrical properties, highlighting the generality of the Skyrmion phase in spiral magnets. Along with the ubiquity of Skyrmion matter comes the challenge of finding means to control and manipulate them, in a device-oriented manner akin to efforts in spintronics community to control the domain wall and vortex motion by electrical current. Spin transfer torque (STT) is a powerful means to induce fast domain wall motion in metallic magnets[7, 8]. Indeed, current-driven Skyrmion rotation[9] and collective drift[10], originating from STT, have been demonstrated in the case of spiral magnets. Theory of current-induced Skyrmion dynamics has been worked out in Refs. [11, 12]. In insulating compounds such as  $\text{Cu}_2\text{OSeO}_3$ , however, the STT-driven mechanism does not work due to the lack of conduction electrons.

As with other magnetically driven multiferroic compounds[13], spiral magnetic order in  $\text{Cu}_2\text{OSeO}_3$  is accompanied by finite electric dipole moment. Recent work by Seki *et al.*[14] further confirmed the mechanism of electric dipole moment induction in  $\text{Cu}_2\text{OSeO}_3$  to be the so-called *pd*-hybridization[15–17]. In short, the *pd*-hybridization mechanism claims the dipole moment  $\mathbf{P}_{ij}$  for every oxygen-TM(transition metal) bond proportional to  $(\mathbf{S}_i \cdot \hat{e}_{ij})^2 \hat{e}_{ij}$  where  $i$  and  $j$  stand for TM and oxygen sites, respectively, and  $\hat{e}_{ij}$  is the unit vector connecting them. Carefully summing up the contributions of such terms over a unit cell consisting of many TM-O bonds, Seki *et al.* were able to deduce the dipole moment distribution associated with a given Skyrmionic spin configuration[14]. It is interesting to note that the numerical procedure performed by Seki *et al.* is precisely the coarse-graining procedure which, in the text-

book sense of statistical mechanics, is tantamount to the Ginzburg-Landau theory of order parameters. Indeed we can show that Seki *et al.*'s result for the dipole moment distribution is faithfully reproduced by the assumption that the local dipole moment  $\mathbf{P}_i$  is related to the local magnetization  $\mathbf{S}_i$  by

$$\mathbf{P}_i = \lambda(S_i^y S_i^z, S_i^z S_i^x, S_i^x S_i^y) \quad (1)$$

with some coupling  $\lambda$ . A similar expression was proposed earlier in Refs. [18, 19] as the GL theory of  $\text{Ba}_2\text{CoGe}_2\text{O}_7$ [20], another known *pd*-hybridization-originated multiferroic material with cubic crystal structure. Each site  $i$  corresponds to one cubic unit cell of  $\text{Cu}_2\text{OSeO}_3$  with linear dimension  $a \sim 8.9\text{\AA}$ , and we have normalized  $\mathbf{S}_i$  to have unit magnitude. The dimension of the coupling constant is therefore  $[\lambda] = \text{C} \cdot \text{m}$ .

Having obtained the proper coupling between dipole moment and the magnetization vector in  $\text{Cu}_2\text{OSeO}_3$  one can readily proceed to study the spin dynamics by solving Landau-Lifshitz-Gilbert (LLG) equation. Very small values of Gilbert damping parameter are assumed in the simulation as we are dealing with an insulating magnet. A new, critical element in the simulation is the term arising from the dipolar coupling

$$H_{\text{ME}} = - \sum_i \mathbf{P}_i \cdot \mathbf{E}_i = - \frac{\lambda}{2} \sum_i \mathbf{S}_i \begin{pmatrix} 0 & E_i^z & E_i^y \\ E_i^z & 0 & E_i^x \\ E_i^y & E_i^x & 0 \end{pmatrix} \mathbf{S}_i, \quad (2)$$

where we have used the magneto-electric coupling expression in Eq. (1). In essence this is a field-dependent (voltage-dependent) magnetic anisotropy term. The total Hamiltonian for spin is given by  $H = H_{\text{HDM}} + H_{\text{ME}}$ , where  $H_{\text{HDM}}$  consists of the Heisenberg and the Dzyaloshinskii-Moriya (DM) exchange and a Zeeman field term. Earlier theoretical studies showed  $H_{\text{HDM}}$  to stabilize the Skyrmion phase[1, 21–24].

Two field orientations can be chosen independently in experiments performed on insulating magnets. First, the direction of magnetic field  $\mathbf{B}$  determines the plane, orthogonal to  $\mathbf{B}$ , in which Skyrmions form. Second, the electric field  $\mathbf{E}$  can be applied to couple to the induced dipole moment of the Skyrmion and used as a “knob” to move it around. Three field directions used in Ref. [14] and the induced dipole moment in each case are classified as (I)  $\mathbf{B} \parallel [001]$ ,  $\mathbf{P} = 0$ , (II)  $\mathbf{B} \parallel [110]$ ,  $\mathbf{P} \parallel [001]$ , and (III)  $\mathbf{B} \parallel [111]$ ,  $\mathbf{P} \parallel [111]$ . One can rotate the spin axis appearing in Eq. (1) accordingly so that the  $z$ -direction coincides with the magnetic field orientation in a given setup and the  $x$ -direction with the crystallographic  $[110]$ . In each of the cases listed above we obtain the magneto-electric coupling, after the rotation,

$$\begin{aligned} H_{\text{ME}}^{(\text{I})} &= -\frac{\lambda}{2} \sum_i E_i ([S_i^y]^2 - [S_i^x]^2), \\ H_{\text{ME}}^{(\text{II})} &= -\frac{\lambda}{2} \sum_i E_i ([S_i^z]^2 - [S_i^x]^2), \\ H_{\text{ME}}^{(\text{III})} &= -\frac{\lambda}{2\sqrt{3}} \sum_i E_i (3[S_i^z]^2 - 1). \end{aligned} \quad (3)$$

In cases (II) and (III) the  $\mathbf{E}$ -field is chosen parallel to the induced dipole moment  $\mathbf{P}$ ,  $\mathbf{E}_i = E_i \hat{\mathbf{P}}$ , to maximize the effect of dipolar coupling. In case (I) where there is no net dipole moment for Skyrmions we chose  $\mathbf{E} \parallel [001]$  to arrive at a simple magneto-electric coupling form shown above.

Suppose now that the  $\mathbf{E}$ -field variation is sufficiently slow on the scale of the lattice constant  $a$  to allow the writing of the continuum energy,

$$H_{\text{ME}} = -\lambda \frac{d}{a} \int d^2 \mathbf{r} E(\mathbf{r}) \rho_{\text{D}}(\mathbf{r}). \quad (4)$$

It is assumed that all variables behave identically along the thickness direction, of length  $d$ . The “dipolar charge” density  $\rho_{\text{D}}(\mathbf{r})$  couples to the electric field  $E(\mathbf{r})$  in the same way as the conventional electric charge does to the potential field in electromagnetism. The analogy is also useful in thinking about the Skyrmion dynamics under the spatially varying  $\mathbf{E}$ -field as we will show. The continuum form of dipolar charge density in Eq. 4 is

$$\begin{aligned} \rho_{\text{D}}^{(\text{I})}(\mathbf{r}_i) &= \frac{1}{2a^2} ([S_i^y]^2 - [S_i^x]^2), \\ \rho_{\text{D}}^{(\text{II})}(\mathbf{r}_i) &= \frac{1}{2a^2} ([S_i^z]^2 - [S_i^x]^2 - 1), \\ \rho_{\text{D}}^{(\text{III})}(\mathbf{r}_i) &= \frac{\sqrt{3}}{2a^2} ([S_i^z]^2 - 1). \end{aligned} \quad (5)$$

Division by the unit cell area  $a^2$  ensures that  $\rho_{\text{D}}(\mathbf{r})$  has the dimension of areal density. Values for the ferromagnetic case,  $S_i^z = 1$ , is subtracted in writing down the definition (5) in order to isolate the motion of the Skyrmion

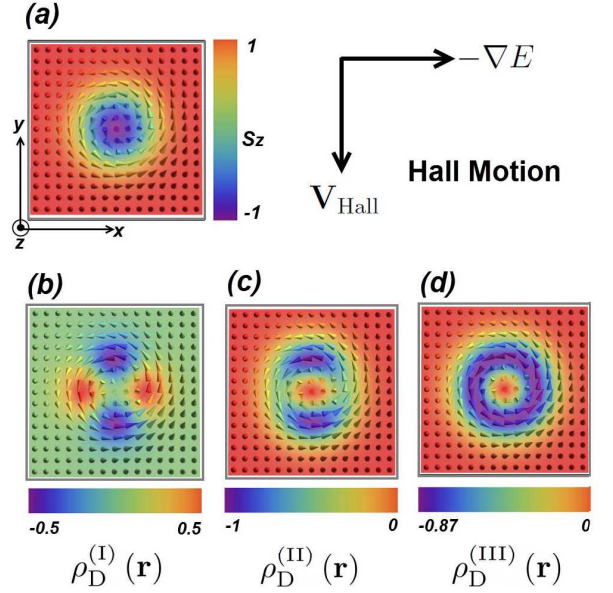


FIG. 1: (color online) (a) Skyrmion configuration and (b)-(d) the corresponding distribution of dipolar charge density for three magnetic field orientations as in Ref. 14. (b)  $\mathbf{B} \parallel [001]$  (c)  $\mathbf{B} \parallel [110]$  (d)  $\mathbf{B} \parallel [111]$ . For each case, electric field is chosen as  $\mathbf{E} \parallel [001]$ ,  $\mathbf{E} \parallel [001]$  and  $\mathbf{E} \parallel [111]$ , respectively. See text for the definition of dipolar charge density. As schematically depicted in (a), the Skyrmion executes a Hall motion in response to electric field gradient.

*relative to the ferromagnetic background.* Due to the subtraction, the dipolar charge is no longer equivalent to the dipole moment of the Skyrmion. The distribution of dipolar charge density for the Skyrmion spin configuration in the three cases are plotted in Fig. 1. In case (I) the total dipolar charge is zero. In cases (II) and (III) the net dipolar charges are both negative with the relation,  $Q_{\text{D}}^{(\text{II})}/Q_{\text{D}}^{(\text{III})} = \sqrt{3}/2$ , where  $Q_{\text{D}}$ , of order unity, is obtained by integrating  $\rho_{\text{D}}(\mathbf{r})$  over the space of one Skyrmion and divide the result by the number of spins  $N_{\text{Sk}}$  inside the Skyrmion. If the field variation is slow on the scale of the Skyrmion, then the point-particle limit is reached by writing  $\rho_{\text{D}}(\mathbf{r}) = Q_{\text{D}} N_{\text{Sk}} \sum_j \delta(\mathbf{r} - \mathbf{r}_j)$  where  $\mathbf{r}_j$  spans the Skyrmion positions, and identical charge  $Q_{\text{D}}$  is assumed for all the Skyrmions. We arrive at the “potential energy” of the collection of Skyrmion particles,

$$H_{\text{ME}} = -\lambda Q_{\text{D}} N_{\text{Sk}} \frac{d}{a} \sum_j E(\mathbf{r}_j). \quad (6)$$

A force acting on the Skyrmion will be given as the gradient  $\mathbf{F}_i = -\nabla_i H_{\text{ME}}$ . Inter-Skyrmion interaction is ignored.

The response of Skyrmions to a given force, on the other hand, is that of an electric charge in strong magnetic field, embodied in the Berry phase action

$(-2\pi S\hbar Q_{\text{Sk}}d/a^3) \sum_j \int dt (\mathbf{r}_j \times \dot{\mathbf{r}}_j) \cdot \hat{z}$ , where  $Q_{\text{Sk}}$  is the quantized Skyrmion charge[12, 25], and  $S$  is the size of spin. Equation of motion follows from the combination of the Berry phase action and Eq. (6),

$$\mathbf{v}_j = \frac{\lambda}{4\pi S\hbar} a^2 N_{\text{Sk}} \frac{Q_{\text{D}}}{Q_{\text{Sk}}} \hat{z} \times \nabla_j E(\mathbf{r}_j), \quad (7)$$

where  $\mathbf{v}_j$  is the  $j$ -th Skyrmion velocity. Typical Hall velocity can be estimated by replacing  $|\nabla E|$  with  $\Delta E/l_{\text{Sk}}$ , where  $\Delta E$  is the difference in the field strength between the left and the right edge of the Skyrmion and  $l_{\text{Sk}}$  is its diameter. Taking  $a^2 N_{\text{Sk}} \sim l_{\text{Sk}}^2$  we find the velocity

$$\frac{\lambda l_{\text{Sk}}}{4\pi S\hbar} \Delta E \sim 10^{-6} \Delta E [\text{m}^2/\text{V} \cdot \text{s}], \quad (8)$$

which gives the estimated drift velocity of 1 mm/s for the field strength difference of  $10^3$  V/m across the Skyrmion. Experimental input parameters of  $l_{\text{Sk}} = 10^{-7}\text{m}$ , and  $\lambda = 10^{-32}\text{C} \cdot \text{m}$  were taken from Ref. [14] in arriving at the estimation, as well as the dipolar and the Skyrmion charges  $Q_{\text{D}} \approx -1$  and  $Q_{\text{Sk}} = -1$ . We may estimate the maximum allowed drift velocity by equating the dipolar energy difference  $\lambda \Delta E$  across the Skyrmion to the exchange energy  $J$ , also corresponding to the formation energy of one Skyrmion[24]. The maximum expected velocity thus obtained is enormous,  $\sim 10^4\text{m/s}$  for  $J \sim 1\text{meV}$ , implying that with the right engineering one can achieve rather high Hall velocity of the Skyrmion. In an encouraging step forward, electric field control of the Skyrmion lattice orientation in the  $\text{Cu}_2\text{OSeO}_3$  crystal was recently demonstrated[26].

Results of LLG simulation is discussed next. To start, a sinusoidal field configuration  $E_i = E_0 \sin(2\pi x_i/L_x)$  is imposed on a rectangular  $L_x \times L_y$  simulation lattice with  $L_x$  much larger than the Skyrmion size. In the absence of Gilbert damping, a single Skyrmion placed in such an environment moved along the “equi-potential line” in the  $y$ -direction as expected from the guiding-center dynamics of Eq. (7). In cases (II) and (III) where the dipolar charges are nonzero the velocity of the Skyrmion drift is found to be proportional to their respective dipolar charges  $Q_{\text{D}}$  as shown in Fig. 2. The drift velocity decreased continuously as we reduced the field gradient, obeying the relation (7) down to the zero velocity limit. The dipolar charge is zero in case (I), and indeed the Skyrmion remains stationary for sufficiently smooth  $\mathbf{E}$ -field gradient. Even for this case, Skyrmions can move for field gradient modulations taking place on the length scale comparable to the Skyrmion radius, for the reason that the forces acting on the positive dipolar charge density blobs (red in Fig. 1(a)) are not completely canceled by those on the negative dipolar charge density blobs (blue in Fig. 1(a)) for sufficiently rapid variations of the

field strength gradient. A small but non-zero drift velocity ensues, as shown in Fig. 2. Longitudinal motion along the field gradient begins to develop with finite Gilbert damping, driving the Skyrmion center to the position of lowest “potential energy”  $E(\mathbf{r})$ . For the Skyrmion lattice, imposing a uniform field gradient across the whole lattice may be too demanding experimentally, unless the magnetic crystal is cut in the form of a narrow strip the width of which is comparable to a few Skyrmion radii. In this case we indeed observe the constant drift of the Skyrmions along the length of the strip in response to the field gradient across it. The drift speed is still proportional to the field gradient, but about an order of magnitude less than that of an isolated Skyrmion under the same field gradient. We observed the excitation of breathing modes of Skyrmions when subject to a field gradient, and speculate that such breathing mode may interfere with the drift motion as the Skyrmions become closed-packed.

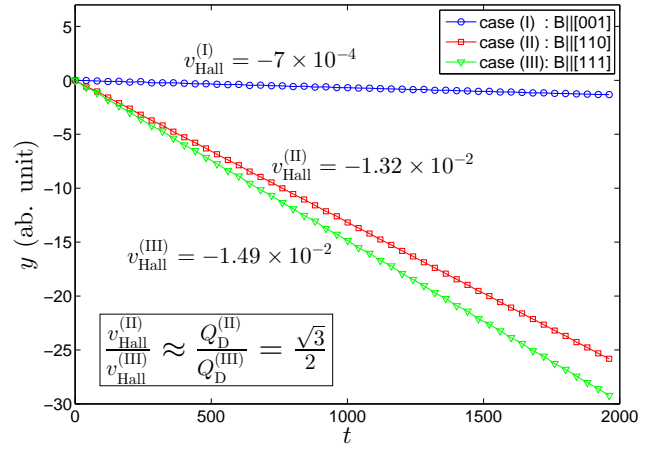


FIG. 2: (color online) Skyrmion position versus time for cases (I) through (III) for sinusoidal electric field modulation (see text) with the Skyrmion center placed at the maximum field gradient position. The average Hall velocities (in arbitrary units) in cases (II) and (III) indicated in the figure are approximately proportional to the respective dipolar charges, in agreement with Eq. (7). A small velocity remains in case (I) due to imperfect cancelation of forces across the dipolar charge profile.

Several movie files are included in the supplementary information. II.gif and III.gif give Skyrmion motion for  $E_i = E_0 \sin(2\pi x_i/L_x)$  on  $L_x \times L_y = 66 \times 66$  lattice for magneto-electric couplings (II) and (III) in Eq. (3). III-Gilbert.gif gives the same  $\mathbf{E}$ -field as III.gif, with finite Gilbert damping  $\alpha = 0.2$ . I.gif describes the case (I) where the average dipolar charge is zero, with a rapidly varying electric field  $E_i = E_0 \sin(2\pi x_i/L_x)$  and  $\lambda_x$  comparable to the Skyrmion radius. The case of a narrow strip with the field gradient across is shown in strip.gif.

Mochizuki’s recent simulation[27] revealed that inter-

nal motion of Skyrmions can be excited with the uniform a.c. magnetic field. Some of his predictions were confirmed by the recent microwave measurement[29]. Here we show that uniform a.c. *electric field* can also excite several internal modes due to the magneto-electric coupling. Time-localized electric field pulse was applied in the LLG simulation and the temporal response  $\chi(t)$  was Fourier analyzed, where the response function  $\chi(t)$  refers to  $(1/2) \sum_i ([S_i^y(t)]^2 - [S_i^x(t)]^2)$ ,  $(1/2) \sum_i ([S_i^z(t)]^2 - [S_i^x(t)]^2)$ , and  $(\sqrt{3}/2) \sum_i [S_i^z(t)]^2$  for cases (I) through (III), respectively. (In Mochizuki's work, the response function was the component of total spin along the a.c. magnetic field direction.)

In case (I), the uniform electric field perturbs the initial cylindrical symmetry of Skyrmion spin profile so that  $\sum_i ([S_i^x(t)]^2 - [S_i^y(t)]^2)$  becomes non-zero and the overall shape becomes elliptical. The axes of the ellipse then rotates counter-clockwise about the Skyrmion center of mass as illustrated in supplementary figure, E-mode.gif. There are two additional modes of higher energies with broken cylindrical symmetry in case (I), labeled X1 and X2 in Fig. 3 and included as X1-mode.gif and X2-mode.gif in the supplementary. The rotational direction of the X1-mode is the same as in E-mode, while it is the opposite for X2-mode.

As in Ref. [27], we find sharply defined breathing modes in cases (II) and (III) at the appropriate resonance frequency  $\omega$ , in fact the same frequency at which the a.c. magnetic field excites the breathing mode. The vertical dashed line in Fig. 3 indicates the common breathing mode frequency. Movie file B1-mode.gif shows the breathing mode in case (III). Additional, higher energy B2-mode (B2-mode.gif) was found in cases (II) and (III), which is the radial mode with one node, whereas the B1 mode is nodeless.

In addition to the two breathing modes, E-mode and the two X-modes are excited in case (II) as well due to the partly in-plane nature of the spin perturbation,  $-(\lambda E(t)/2) \sum_i ([S_i^z(t)]^2 - [S_i^x(t)]^2)$ . In contrast, case (III), where the perturbation  $-(\sqrt{3}\lambda E(t)/2) \sum_i [S_i^z(t)]^2$  is purely out-of-plane, one only finds the B-modes. As a result, case (I) and (III) have no common resonance modes or peaks, while case (II) has all the peaks (though X1 and X2 peaks are small). Compared to the magnetic field-induced resonances, a richer variety of modes are excited by a.c. electric field. In particular, the E-mode has lower excitation energy than the B-mode and has a sharp resonance feature, which should make its detection a relatively straightforward task. Full analytic solution of the excited modes[28] will be given later.

In summary, motivated by the recent discovery of magneto-electric material  $\text{Cu}_2\text{OSeO}_3$  exhibiting Skyrmion lattice phase, we have outlined the theory of Skyrmion dynamics in such materials. Electric field gradient is identified as the source of Skyrmion Hall motion.

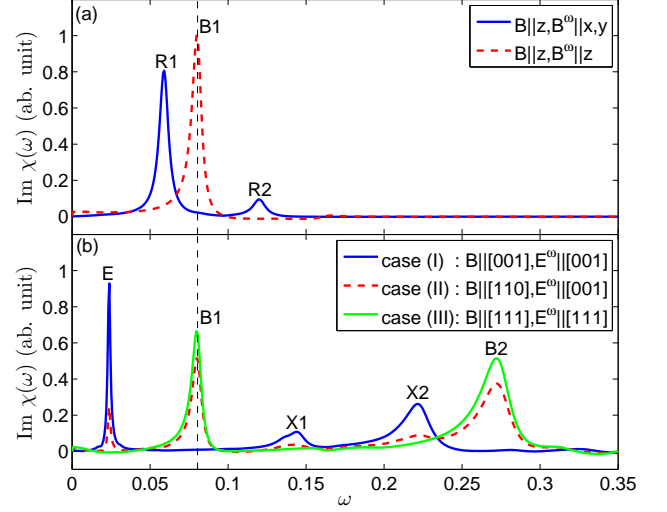


FIG. 3: (color online) (a) Absorption spectra for a.c. uniform magnetic field as in Mochizuki's work (reproduced here for comparison). (b) Absorption spectra for a.c. uniform electric field in cases (I) through (III). In case (I) where there is no net dipolar charge we find three low-energy modes E, X1, and X2. For case (III) where the dipolar charge is finite we find B1 and B2 radial modes excited. Case (II) exhibits all five modes. Detailed description of each mode is given in the text.

Several resonant excitations by a.c. electric field are identified.

J. H. H. is supported by NRF grant (No. 2010-0008529, 2011-0015631). Y. Q. L. is supported by NSFC (Grant No. 11074216). J. H. H. acknowledges earlier collaboration with N. Nagaosa, Youngbin Tchoe, and J. Zang on a related model and informative discussion with Y. Tokura.

\* Electronic address: hanjh@skku.edu

- [1] S. Mühlbauer, B. Binz, F. Jonietz, C. Pfleiderer, A. Rosch, A. Neubauer, R. Georgii, and P. Böni, *Science* **323**, 915 (2009).
- [2] W. Münzer, A. Neubauer, T. Adams, S. Mühlbauer, C. Franz, F. Jonietz, R. Georgii, P. Böni, B. Pedersen, M. Schmidt, A. Rosch, and C. Pfleiderer, *Phys. Rev. B* **81**, 041203(R) (2010).
- [3] X. Z. Yu, Y. Onose, N. Kanazawa, J. H. Park, J. H. Han, Y. Matsui, N. Nagaosa, and Y. Tokura, *Nature* **465**, 901 (2010).
- [4] X. Z. Yu, N. Kanazawa, Y. Onose, K. Kimoto, W. Z. Zhang, S. Ishiwata, Y. Matsui, and Y. Tokura, *Nature Mat.* **10**, 106 (2011).
- [5] N. Kanazawa, Y. Onose, T. Arima, D. Okuyama, K. Ohoyama, S. Wakimoto, K. Kakurai, S. Ishiwata, and Y. Tokura, *Phys. Rev. Lett.* **106**, 156603 (2011).
- [6] S. Seki, X. Z. Yu, S. Ishiwata, and Y. Tokura, *Science*

- 336**, 198 (2012).
- [7] G. Tatara, H. Kohno, and J. Shibata, Phys. Rep. **468**, 213 (2008).
  - [8] D. C. Ralph and M. Stiles, J. Magn. Mag. Mat. **320**, 1190 (2008).
  - [9] F. Jonietz, S. Mühlbauer, C. Pfleiderer, A. Neubauer, W. Münzer, A. Bauer, T. Adams, R. Georgii, P. Böni, R. A. Duine, K. Everschor, M. Garst, and A. Rosch, Science **330**, 1648 (2010).
  - [10] T. Schulz, R. Ritz, A. Bauer, M. Halder, M. Wagner, C. Franz, C. Pfleiderer, K. Everschor, M. Garst, and A. Rosch, Nat. Phys. **8**, 301 (2012).
  - [11] K. Everschor, M. Garst, R. A. Duine, and A. Rosch, Phys. Rev. B **84**, 064401 (2011).
  - [12] J. Zang, M. Mostovoy, J. H. Han, and N. Nagaosa, Phys. Rev. Lett. **107**, 136804 (2011).
  - [13] Y. Tokura and S. Seki, Adv. Mat. **21**, 1 (2009).
  - [14] S. Seki, S. Ishiwata, and Y. Tokura, arXiv:1206.4404v1 (2012).
  - [15] Chenglong Jia, Shigeki Onoda, Naoto Nagaosa, and Jung Hoon Han, Phys. Rev. B **74**, 224444 (2006).
  - [16] Chenglong Jia, Shigeki Onoda, Naoto Nagaosa, and Jung Hoon Han, Phys. Rev. B **76**, 144424 (2007).
  - [17] Taka-hisa Arima, J. Phys. Soc. Jpn. **76**, 073702 (2008).
  - [18] Judit Romhányi, Miklós Lajkó, and Karlo Penc, Phys. Rev. B **84**, 224419 (2011).
  - [19] J. H. Han, unpublished note.
  - [20] H. Murakawa, Y. Onose, S. Miyahara, N. Furukawa, and Y. Tokura, Phys. Rev. Lett. **105**, 137202 (2010).
  - [21] A. N. Bogdanov and D. A. Yablonskii, Sov. Phys. JETP **68**, 101 (1989); A. Bogdanov and A. Hubert, J. Magn. Mater. **138**, 255 (1994).
  - [22] U. K. Roßler, A. N. Bogdanov, and C. Pfleiderer, Nature **442**, 797 (2006).
  - [23] Su Do Yi, Shigeki Onoda, Naoto Nagaosa, and Jung Hoon Han, Phys. Rev. B **80**, 054416 (2009).
  - [24] Jung Hoon Han, Jiadong Zang, Zhihua Yang, Jin-Hong Park, and Naoto Nagaosa, Phys. Rev. B **82**, 094429 (2010).
  - [25] Michael Stone, Phys. Rev. B **53**, 16573 (1996).
  - [26] J. S. White, *et al.* arXiv:1208.1146 (2012).
  - [27] Masahito Mochizuki, Phys. Rev. Lett. **108**, 017601 (2012).
  - [28] Olga Petrova and Oleg Tchernyshyov, Phys. Rev. B **84**, 214433 (2011); Imam Makhfudz, Benjamin Krüger, and Oleg Tchernyshyov, arXiv:1208.3123 (2012).
  - [29] Y. Onose, Y. Okamura, S. Seki, S. Ishiwata, and Y. Tokura, Phys. Rev. Lett. **109**, 037603 (2012).